LEARNING TO ACT FROM ACTIONLESS VIDEOS THROUGH DENSE CORRESPONDENCES

Anonymous authors
Paper under double-blind review

ABSTRACT

In this work, we present an approach to construct a video-based robot policy capable of successfully executing diverse tasks across different robots and environments from few video demonstrations without using any action annotations. Our method leverages images as a task-agnostic representation, encoding both the state and action information, and text as a general representation for specifying robot goals. By synthesizing videos that "hallucinate" robot executing actions and in combination with dense correspondences between frames, our approach can infer the closed-formed action to execute to an environment without the need of *any* explicit action labels. This unique capability allows us to train the policy solely based on RGB videos and deploy learned policies to various robotic tasks. We demonstrate the efficacy of our approach in learning policies on table-top manipulation and navigation tasks. Additionally, we contribute an open-source framework for efficient video modeling, enabling the training of high-fidelity policy models using just 4 GPUs within a single day.

1 INTRODUCTION

A goal of robot learning is to construct a policy that can successfully and robustly execute diverse tasks across various robots and environments. A major obstacle is the diversity present in different robotic tasks. The state representation necessary to fold a cloth differs substantially from the one needed for pouring water, picking and placing objects, or navigating, requiring a policy that can process each state representation which arises. Furthermore, the action representation to execute each task varies significantly subject to differences in motor actuation, gripper shape, and task goals, requiring a policy that can correctly deduce an action to execute across different robots and tasks.

One possible solution is to use images as a task-agnostic method for encoding both the states and the actions to execute. In this setting, policy prediction involves synthesizing a video that depicts the actions a robot should execute (Du et al., 2023; Finn & Levine, 2017; Kurutach et al., 2018). However, directly predicting an image representation a robot should execute does not explicitly encode the required robot actions to execute. To address this, past works either learn an action-specific video prediction model (Finn & Levine, 2017) or a task-specific inverse-dynamics model to regress actions from videos (Du et al., 2023). Both approaches rely on task-specific action labels, preventing general policy prediction across different robot tasks.

In this work, we present a method that can directly regress actions from video predictions without requiring *any* action labels or task-specific inverse-dynamics model. This enables us to directly *reformulate* policy learning as an *equivalent* text-conditioned video generation problem. To infer actions from video, we leverage dense correspondences between two adjacent frames of a synthesized video to *implicitly* capture the action transform necessary to move from one frame to the next and obtain the action to execute. Given inferred transforms, we can then directly use off-the-shelf inverse kinematics and motion planners to robustly infer actions across environments without any explicit action labels. We illustrate the efficacy of using such an action regression technique across various tasks such as table-top assembly, ego-centric object navigation, and real-world robot manipulation in Fig. 1.

Another limitation of existing approaches that formulate policy prediction as a video prediction problem is that they suffer from high computational costs during training, requiring the use of over 256 TPU pods (Du et al., 2023), with limited availability of the underlying source code. As a contribution, we provide an open-source codebase for training video policy models. Through a series

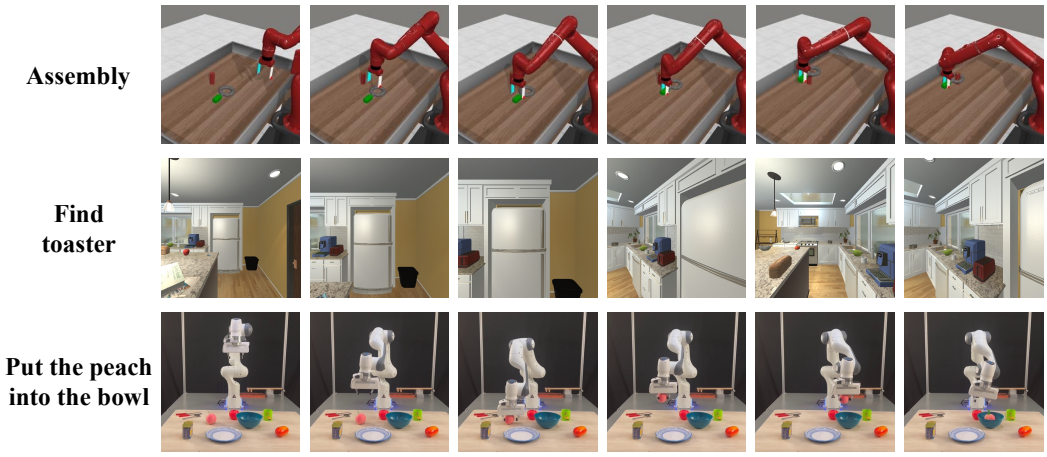

Figure 1: **Diverse Task Execution without Action Labels.** Our approach can execute policies given only synthesized video, without any action labels, across various manipulation, navigation, and real-world tasks.

of architectural optimizations, our framework enables the generation of high-fidelity videos for policy execution, with training accomplished on just 4 GPUs in a single day.

Concretely, we contribute the following: **(1)** We propose to method to infer actions from video prediction without the need of *any action labels* by leveraging dense correspondences in a video. **(2)** We illustrate how this approach enables us to learn policies that can solve diverse tasks across both table-top manipulation and navigation by directly formulating policy generation as a text-conditioned generation problem. **(3)** We present an open-source framework which enables efficient video modeling that enables us to train policies efficiently on 4 GPUs in a single day.

2 Related Work

Robot learning from videos. A large body of work has explored how to leverage videos for effective robot learning (Pari et al., 2022; Nair et al., 2022a; Shao et al., 2021; Chen et al., 2021; Bahl et al., 2022; Sharma et al., 2019; Lee & Ryoo, 2017; Du et al., 2023). One approach relies upon using existing video datasets to construct effective visual representations (Pari et al., 2022; Nair et al., 2022a). Alternatively, goal or subtask information for robotic execution may be extracted for videos (Shao et al., 2021; Chen et al., 2021; Bahl et al., 2022; Sharma et al., 2019; Lee & Ryoo, 2017; Sivakumar et al., 2022) or used as a dynamics model for planning (Finn & Levine, 2017; Kurutach et al., 2018). Most similar to our work, in UniPi (Du et al., 2023), policy prediction may directly be formulated as a text-conditioned video generation problem. Our approach extends the approach in UniPi and illustrates how dense correspondences enable action inference without any explicit action labels.

Dense Correspondences. Dense correspondences have emerged as an effective implicit parameterization of actions and poses (Florence et al., 2018; Manuelli et al., 2022; Yen-Chen et al., 2022; Simeonov et al., 2022; 2023; Chun et al., 2023; Sundaresan et al., 2020; Ryu et al., 2023). Given dense correspondences in 2D (Florence et al., 2018; Manuelli et al., 2022; Sundaresan et al., 2020; Yen-Chen et al., 2022) of 3D (Simeonov et al., 2022; 2023; Chun et al., 2023; Ryu et al., 2023) both object and manipulator poses may be inferred by solving for rigid transforms given correspondences. Our approach uses dense correspondences between adjacent frames of synthesized videos to calculate object of scene transformations and then infer robot actions.

Learning from Observation. In contrast to imitation learning (*i.e.*, learning from demonstration) Osa et al. (2018); Kipf et al. (2019); Ding et al. (2019); Fang et al. (2019); Wang et al. (2023), which assumes access to expert actions, learning from observation methods (Torabi et al., 2019b; 2018; 2019a; Lee et al., 2021; Karnan et al., 2022) learn from expert state sequences (*e.g.*, video frames). Action-free pre-training methods (Baker et al., 2022; Escontrela et al., 2023) extract knowledge from unlabeled videos and learn target tasks through RL. Despite encouraging results, these methods require interacting with environments, which may be expensive or even impossible. In contrast, our proposed method does not require environmental interactions.

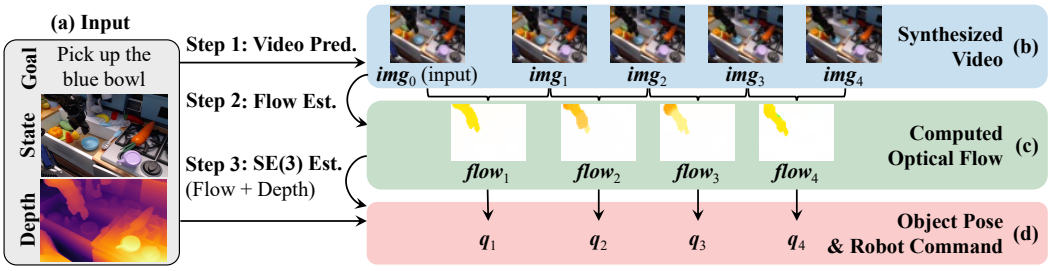

Figure 2: **Overall framework of AVDC.** (a) Our model takes the RGBD observation of the current environmental state and a textual goal description as its input. (b) It first synthesizes a video of *imagined* execution of the task using a diffusion model. (c) Next, it estimates the optical flow between adjacent frames in the video. (d) Finally, it leverages the optical flow as dense correspondences between frames and the depth of the first frame to compute $SE(3)$ transformations of the target object, and subsequently, robot arm commands.

3 Action from Video Dense Correspondences

Yilun one thing to check wrt to the method section is if other past video diffusion model papers have also used the factorized resnet block. I think Imagen video might have used it

The architecture of our proposed framework, Action from Video Dense Correspondences (AVDC), is depicted in Fig. 2. AVDC consists of three modules. Given the initial observation (*i.e.*, an RGBD image of the scene and a textual task description), we first employ a video synthesis model to generate a video that implicitly captures the sequence of required actions (Section 3.1). Then, we use a flow prediction model to estimate the optical flow of the scene and objects from the synthesized video (Section 3.2). Finally, leveraging the initial depth map and predicted optical flows, we reconstruct the movements of objects for manipulation or robots for navigation, described in Section 3.3.

3.1 Text-Conditioned Video Generation

Our text-conditioned video generation model is a conditional diffusion model. The diffusion model takes the initial frame and a text description as its condition and learns to model the distribution of possible future frames. Throughout this paper, our video generation model predicts a fixed number of future frames ($T = 8$ in our experiments).

The diffusion model aims to approximate the distribution $p(img_{1:T}|img_0, txt)$, where $img_{1:T}$ represents the video frames from time step 1 to T, img_0 denotes the initial frame, and txt represents the task description. We train a denoising function ϵ_θ that predicts the noise applied to $img_{1:T}$ given the perturbed frames. Given the Gaussian noise scheduling β_t, our overall objective is,

$$\mathcal{L}_{\text{MSE}} = \left\| \epsilon - \epsilon_\theta \left(\sqrt{1-\beta_t} img_{1:T} + \sqrt{\beta_t}\epsilon, t \mid txt \right) \right\|^2,$$

where ϵ is sampled from a multivariate standard Gaussian distribution, and t is a randomly sampled diffusion step t. A main practical challenge with training such video diffusion models is that they are usually computationally expensive. For example, the closest work to us, Unipi (Du et al. (2023)), requires over 256 TPU pods to train. In this paper, we build a high-fidelity video generation model that can be trained on 4 GPUs in a single day through a series of architectural optimizations.

Our model is a modified version of the image diffusion model proposed by Dhariwal & Nichol (2021), built upon U-Net (Ronneberger et al., 2015), as illustrated in Fig. 3a. We adopt a spatial resolution of 64 by 64 in our model. The U-Net consists of 4 downsample blocks followed by 4 upsample blocks. To enhance consistency with the initial frame, we concatenate the input condition frame img_0 to all future frames $img_{1:T}$. To encode the text, we use a CLIP-Text (Radford et al., 2021) encoder to obtain a vector embedding and combine it into the video generative model as additional inputs to individual downsampling and upsampling blocks.

Importantly, we use a factorized spatial-temporal convolution (Ho et al., 2022) within each ResNet block (He et al., 2016). As shown in Fig. 3b, in our approach, the 5D input feature map with shape (B, H, W, T, C), where B is the batch size, H and W represent the spatial dimensions, T is the number of time frames, and C denotes the number of channels, undergoes two consecutive convolution operations. First, we apply a spatial convolution identically and independently to each time step $t = 1, 2, \cdots, T$. Then, we employ a temporal convolution layer identically and independently at each spatial location. This factorized spatial-temporal convolution replaces conventional 3D convolution

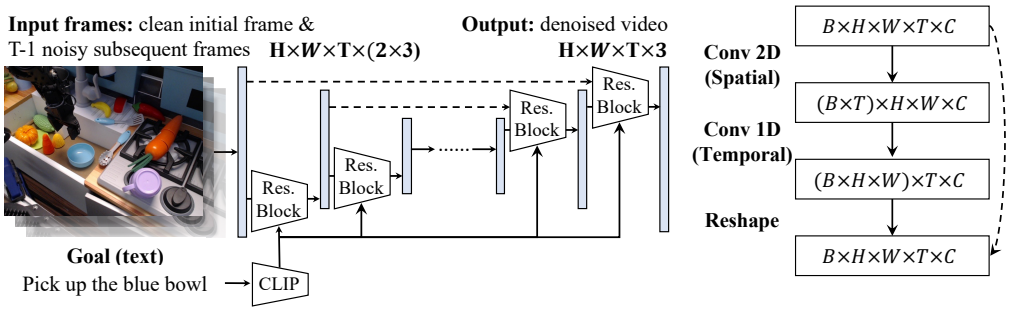

(a) U-Net architecture for our base diffusion model (b) Factorized spatial-temporal ResNet block

Figure 3: **Network architecture of our video diffusion model.** (a) We use an U-Net architecture following Dhariwal & Nichol (2021) but extending it to videos. (b) We use a factorized spatial-temporal convolution kernel Sun et al. (2015) as the basic building block. Dashed lines in both figures represent residual connections (He et al., 2016).

methods, leading to significant improvements in training and inference efficiency without sacrificing generation quality.

3.2 Flow Prediction

To regress actions from predicted videos, we leverage flow prediction as an intermediate representation. We employ off-the-shelf GMFlow, a transformer architecture specifically designed for optical flow prediction (Xu et al., 2022). Given two consecutive frames img_i and img_{i+1} predicted by the video diffusion model, GMFlow predicts the optical flow between two images as a vector field on the image, which is essentially a pixel-level *dense correspondence map* between two frames. This allows us to track the movement of each input pixel with a simple integration of this vector field over time.

Alternatively, one could train diffusion models to directly predict the flow by first preprocessing training videos with the flow prediction model. However, in our experiments, we encountered challenges in optimizing such models and observed that they failed to match the performance achieved by the two-stage inference pipeline. We conjecture that this difficulty arises from the lack of spatial and temporal smoothness in flow fields. For instance, the flow field is sparse when only a single object moves. Consequently, the Gaussian diffusion model may not be the optimal modelling for flow distributions. We empirically compare two alternatives in subsequent experiments.

3.3 Action Regression from Flows and Depths

Based on the predicted flow, which essentially gives us a dense prediction of pixel movements, we can reconstruct object movements and robot movements in the video. Our key insight is to, given the 3D information (depth) of the input frame and dense pixel tracking, reconstruct a sequence of 3D rigid transformations for each object. In this work, we explore two different settings: predicting object transformations assuming a fixed camera (fixed-camera object manipulation) and predicting camera (robot) movement assuming a static scene (visual navigation).

Predict object-centric motion.. We first consider predicting 3D object motions in videos assuming a fixed camera. We represent each object as a set of 3D points $\{x_i\}$. Given the camera intrinsic matrix and the input RGBD image, we can compute the initial 3D positions of these points. Let T_t denote the rigid body transformation of the object at time step t relative to the initial frame. We can express the projection of a 3D point onto the image plane at time step t as $KT_tx = (u_t, v_t, d_t)$, where K is the camera intrinsic matrix. Furthermore, the projected 2D point on frame t is thus $(u_t/d_t, v_t/d_t)$.

The optical flow tracking provides us with the projection of the same point in frame t, specifically u_t/d_t and v_t/d_t. By tracking all points in $\{x_i\}$, we can find the optimal transformation T_t that minimizes the following L2 loss:

$$\mathcal{L}_{\text{Trans}} = \sum_i \left\| u_t^i - \frac{(KT_tx_i)_1}{(KT_tx_i)_3} \right\|_2^2 + \left\| v_t^i - \frac{(KT_tx_i)_2}{(KT_tx_i)_3} \right\|_2^2,$$

where (u_t^i, v_t^i) is the corresponding pixel of point x_i in frame t, and $(KT_tx_i)_i$ denotes the i-th entry of the vector. It's worth noting that even if we do not directly observe d_t, this loss function remains well-formed based on the assumption that T_t represents a rigid body transformation.

During execution, we first extract the mask of the object to manipulate and use the dense correspondences in predicted videos to compute the sequence of rigid body transformations for the object.

(a) Meta-World (b) iTHOR (c) Bridge Dataset (d) Franka Emika

Figure 4: **Environments & Tasks. (a) Meta-World** is a simulated benchmark featuring various tasks with a Sawyer robot arm. **(b) iTHOR** is a simulated benchmark for embodied common sense reasoning. We adopt its object navigation task, which requires navigating to target objects located in different rooms. **(c) Bridge** is a real-world video dataset comprised of 33,078 teleoperated robot demonstrations conducting various kitchen tasks. **(d) Real-World Franka Emika** is a pick-and-place tabletop environment with a Franka Emika robot arm.

Next, given inferred object transformations, we can use existing off-the-shelf robotics primitives to generalizably infer actions in the environment. In particular, if the object is graspable, we randomly sample a grasp on the object and then compute the target robot end-effector pose based on the target object pose and the grasping pose. When the object is not directly graspable (*e.g.*, a door), we similarly sample a contact point and use a push action to achieve the target object transformation.

We treat the grasp/contact point as the first subgoal. Then, we iteratively apply the computed transformation on the current subgoal to compute the next subgoal until all subgoals are computed. Next, we use a position controller to control the robot to reach the subgoals one by one. More details on inferring robot manipulation actions can be found in Section F. In contrast to our approach, directly learning explicitly regress actions using a learned inverse dynamics requires a substantial number of action labels so that a neural network can learn existing knowledge such as inverse dynamics, grasping and motion-planning.

Inferring Robot Motion. The similar algorithm can also be applied to predict robot (*i.e.*, the camera) motion assuming all objects are static. Due to the duality of camera motion and object motion, we can use exactly the same optimization algorithm to find T_t (object-centric motion), and the camera motion $C_t = (T_t)^{-1}$. Concretely, we make the following modifications to adapt AVDC to navigation tasks. (1) The video diffusion model is trained to duplicate the last frame once the object is found. (2) Instead of tracking objects, we utilize the optical flow of the whole frame to estimate the rigid transformations between frames. (3) Based on the calculated rigid transformations, we simply map the transformations to the closest actions, detailed in Section G.

Depth Estimation. We can reconstruct 3D object or robot trajectories solely from the depth map of the initial frame (*i.e.*, the subsequent depth maps is not required). By leveraging dense correspondences between frames and assuming rigid object motion, we can reconstruct accurate 3D trajectories. This holds significant advantages as it enables us to train video prediction models exclusively using RGB videos, allowing for learning from online sources like YouTube, and only requires an RGB-D camera (or monocular depth estimator) at execution time. By eliminating the dependence on depth maps from subsequent frames, our system is significantly more adaptable to various data sources.

Replanning Strategy. After inferring the object or robot trajectories, we can execute the trajectory using a position controller in an open-loop manner. Yet, it can suffer from accumulated errors. As the planning horizon increases, the accuracy of predicted object locations diminishes due to combined errors in video synthesis and flow prediction. To mitigate this issue, we propose a replanning strategy. If the robot movement is smaller than 1mm over 15 consecutive time steps while the task has not been fulfilled, we re-run our video generation and action prediction pipeline from the current observation.

4 Experiment

We describe the baselines and the variants of our method AVDC in Section 4.1. Then, we compare AVDC to its variants and the baselines systematically on simulated robot arm manipulation tasks in Meta-World (Fig. 4a) and navigation tasks in iTHOR (Fig. 4b). Although it is possible to obtain ground-truth robot actions for demonstrations in these two datasets, we did not consider using them for our method. We leverage the Bridge dataset (Fig. 4c) and evaluate AVDC on real-world manipulation tasks with a Franka Emika robot arm (Fig. 4d).

	door-open	door-close	basketball	shelf-place	btn-press	btn-press-top
BC-Scratch	21.3%	36.0%	0.0%	0.0%	34.7%	12.0%
BC-R3M	1.3%	58.7%	0.0%	0.0%	36.0%	4.0%
UniPi (With Replan)	0.0%	36.0%	0.0%	0.0%	6.7%	0.0%
AVDC (ID)	0.0%	36.0%	0.0%	0.0%	0.0%	0.0%
AVDC (Flow)	0.0%	0.0%	0.0%	0.0%	1.3%	**40.0%**
AVDC (No Replan)	30.7%	28.0%	21.3%	8.0%	34.7%	17.3%
AVDC (Full)	**72.0%**	**89.3%**	**37.3%**	**18.7%**	**60.0%**	24.0%
	faucet-close	faucet-open	handle-press	hammer	assembly	**Overall**
BC-Scratch	18.7%	17.3%	37.3%	0.0%	1.3%	16.2%
BC-R3M	18.7%	22.7%	28.0%	0.0%	0.0%	15.4%
UniPi (With Replan)	4.0%	9.3%	13.3%	4.0%	0.0%	6.1%
AVDC (ID)	4.0%	9.3%	13.3%	4.0%	0.0%	6.1%
AVDC (Flow)	42.7%	0.0%	66.7%	0.0%	0.0%	13.7%
AVDC (No Replan)	12.0%	17.3%	41.3%	0.0%	5.3%	19.6%
AVDC (Full)	**53.3%**	**24.0%**	**81.3%**	**8.0%**	**6.7%**	**43.1%**

Table 1: **Meta-World Result.** We report the mean success rate across tasks. Each entry of the table shows the average success rate aggregated from 3 camera poses with 25 seeds for each camera pose.

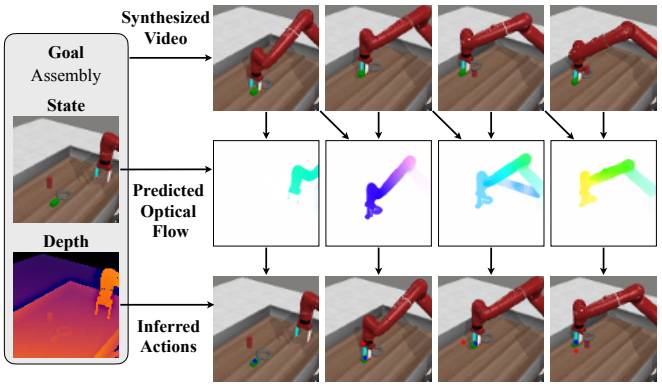

Figure 5: **Qualitative Results on Meta-World.** AVDC can reliably synthesize a video, predict optical flow between frames, and infer and execute actions to fulfill the assembly task. Current subgoals (•) and next subgoals (•) are rendered in inferred action visualizations.

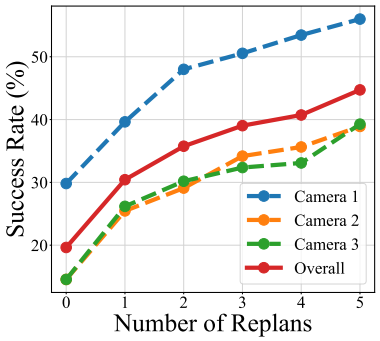

Figure 6: **Number of Replanning Steps vs. Success Rate.** AVDC achieves higher success with more replanning trials, justifying the effectiveness of our replanning strategy.

4.1 Baselines and Variants of AVDC

Baselines. We compare AVDC to a multi-task behavioral cloning (BC) baseline given access to a set of expert actions from all videos (15216 labeled frame-action pairs in Meta-World and 5757 in iTHOR), which are unavailable to our method. This baseline encodes the RGB observation to a feature vector with a ResNet-18 (He et al., 2016). Then, the feature vector is concatenated with a one-hot encoded camera ID and a task representation encoded by the CLIP-Text model (Radford et al., 2021). The concatenated representation is then fed to a 3-layer MLP, which produces an action. We explore initializing the weights of ResNet-18 from scratch (BC-Scratch) or from the pre-trained parameters of R3M (Nair et al., 2022b) (BC-R3M).

We also compare AVDC with UniPi (Du et al., 2023), which is an action-learning-from -video method that leverages a learned inverse dynamics model in the environment to generate actions from videos. Since the exact number of steps between two generated frames in our model may vary across different episodes (because we generate a fixed number of 8 frames for each episode), we slightly modify the basic inverse dynamics model to output an additional binary label indicating whether to switch to the next frame of video plan. This additional binary predictor can be trained from the existing data we used to train the BC policy; therefore we use the same dataset as our BC experiments for fair comparison.

AVDC and its Variants. We compare AVDC to other approaches to predict dense correspondence.

- **AVDC (Flow)** learns to directly predict the optical flow between frames as described in Section 3.2. We include this variant to justify our 2-stage design, which synthesizes a video and then infers optical flows between each pair of frames.

- **AVDC (No Replan)** is the opened-loop variant of our proposed method, which synthesizes a video, infers flows, produces a plan, executes it, and finishes, regardless of if it fails or succeeds. We include this variant to investigate whether our replanning strategy is effective.
- **AVDC (Full)** is our proposed method in full, employing the 2-stage design and can replan.

We have also included additional ablation studies on the effect of first-frame conditioning in video generation, and different text encoders in the Appendix.

4.2 META-WORLD

Setup. Meta-World (Yu et al., 2019) is a simulated benchmark which features various manipulation tasks with a Sawyer robot arm. We include 11 tasks, and for each task, we render videos from 3 different camera poses. We collect 5 demonstrations per task per camera position, resulting in 165 videos in total.

Each policy is evaluated on each task with 3 camera poses, each with 25 trials. A policy succeeds if it reaches the goal state within the maximum environment step and fails otherwise. The positions of the robot arm and objects are randomized when each episode begins. The result is reported in Table 1.

Comparison to BC. Our method AVDC (Full) consistently outperforms the two BC baselines (BC-Scratch and BC-R3M) on all the tasks by a large margin. This indicates that the tasks are still very challenging, even with access to expert actions.

Comparing AVDC Variants. AVDC (Flow) performs the best on button-press-topdown and achieves reasonable performance on faucet-close and handle-press, while performing very poorly on the rest of the tasks. As described in Section 3.2, the diffusion model employed in this work may not be optimal for flow prediction. Also, AVDC (Full) consistently outperforms AVDC (No Replan), justifying the effectiveness of our closed-loop design, enabling replanning when the policy fails.

Intermediate Outputs. To provide insights into the pipeline of AVDC, we visualized the synthesized video, predicted optical flow, and inferred actions (*i.e.*, motion planning) in Fig. 5. Our diffusion model synthesizes a reasonable video showing the robot arm picking up the nut and placing it onto the peg. The optical flow predicted from video frames accurately captures the robot arm's motions. Then, based on the predicted flow, the inferred actions can reliably guide the arm to fulfill the task.

Effect of Replanning Trials. We investigate how varying the maximum number of planning affects the performance of AVDC. As presented in Fig. 6, the success rate consistently increases with more replanning trials, demonstrating the effectiveness of our proposed replanning strategy.

Failure Modes. The primary failure mode we observed is the errors made by the optical flow tracking model, partially because these models are not trained on any in-domain data. Since the prediction resolution is not very high in our experiments, small pixel-level errors in tracking small objects would result in large errors in the 3D space. We believe that by directly increasing the resolution of video synthesis or by training an in-domain optical flow model, we can improve the performance.

4.3 ITHOR

Setup. iTHOR (Kolve et al., 2017) is a simulated benchmark for embodied common sense reasoning. We consider the object navigation tasks for evaluation, where an agent randomly initialized into a scene learns to navigate to an object of a given type (*e.g.*, toaster, television). At each time step, the agent observes a 2D scene and takes one of the four actions: `MoveForward`, `RotateLeft`, `RotateRight`, and `Done`. We chose 12 different objects to be placed at 4 type of rooms (*e.g.*, kitchen, living room).

Each policy is evaluated on 12 object navigation tasks distributed in 4 different types of rooms (3 tasks for each room). A policy succeeds if the target object is in the agent's sight and within a 1.5m distance within the maximum environment step or when `Done` is predicted and fails otherwise. The position of the agent is randomized at the beginning of each episode. The result is reported in Table 2.

Comparison to BC. Our proposed method AVDC can find target objects in different types of rooms fairly often (31.3%), while the two BC baselines fail entirely. BC-R3M with a pre-trained ResNet-18 performs worse than BC-Scratch, which can be attributed to the fact that R3M is pre-trained on robot manipulation tasks and might not be suitable for visual navigation tasks.

Intermediate Outputs. The intermediate outputs produced by AVDC are presented in Fig. 7. The diffusion model can synthesize video showing an agent navigating to the target object. Then, desired agent movements can be easily inferred from the predicted optical flow, resulting in the

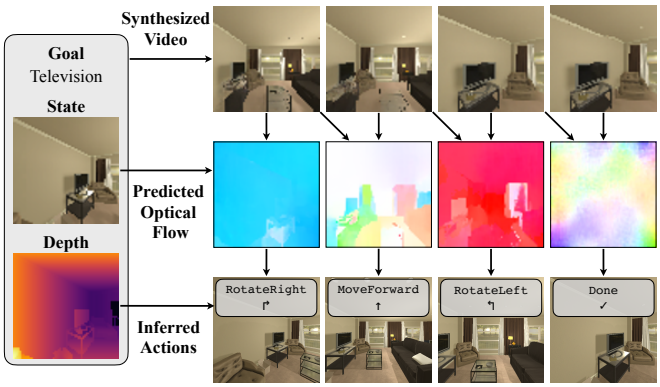

Figure 7: **Qualitative Results on iTHOR.** AVDC can reliably synthesize a video, predict optical flow between frames, and infer and execute actions to navigate to the television.

Room	BC-Scratch	BC-R3M	AVDC
Kitchen	1.7%	0.0%	**26.7%**
Living Room	3.3%	0.0%	**23.3%**
Bedroom	1.7%	1.7%	**38.3%**
Bathroom	1.7%	0.0%	**36.7%**
Overall	2.1%	0.4%	**31.3%**

Table 2: **iTHOR Result.** We report the mean success rate, aggregated from 3 types of objects per room with 20 episodes per object. Both the two BC baselines fail to achieve meaningful performance on the iTHOR object navigation tasks. On the other hand, AVDC performs reasonably with a 31.3% average success rate.

ease of mapping the flow to `MoveForward`, `RotateLeft`, or `RotateRight`. When no flow is predicted, it indicates the agent has found the object and selects `Done` as the predicted action.

4.4 Cross-Embodiment Learning from Human Videos

To demonstrate the ability of our method to learn robotics tasks from out-of-domain videos without natural actions, we applied our method to the State Pusher task introduced in Schmeckpeper et al. (2021); Zakka et al. (2022). Specifically, we trained a video diffusion model on only human pushing data, which does not contain any action labels. Then, we tested the model on the generalization of the learned policy directly on the simulated robot pushing task *without any fine-tuning*. Our model exhibits strong zero-shot transfer capability, achieving a 90% zero-shot successful rate out of 40 runs. We illustrate videos of rendered videos in simulation and the associated policy on our website. Note that in this environment, there are no convenient pre-programmed scripted policies that can be used to collect demonstrations as in MetaWorld; therefore, actions from expert demonstrations are not available. We used the same U-net architecture as used in MetaWorld experiments and trained the model for 10k steps (4 hours) on 198 human-pushing videos.

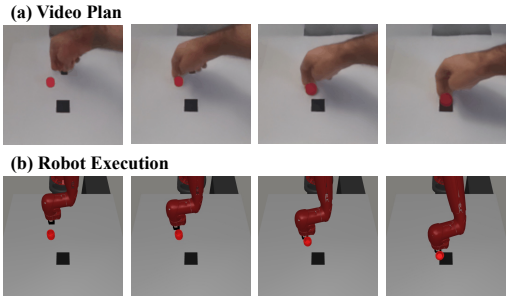

Figure 8: **Qualitative Results on the State Pusher task.** AVDC learns to synthesize video plans (a) by watching human actions and generates actions in the simulated environments (b), *without any fine-tuning*.

4.5 Real-World Franka Emika Robot Arm with Bridge Dataset

The flexibility of our proposed framework AVDC allows us to directly learn robot policies from real-world videos. In particular, we train our video generation model on the Bridge dataset, and perform evaluation on a real-world tabletop manipulation environment.

Setup. The Bridge dataset (Ebert et al., 2022) provides 33,078 teleoperated WidowX 250 robot demonstrations of various kitchen tasks captured by a web camera without depth information. Our real-world setup comprises a Franka Emika robot arm and an Intel Realsense D435 RGBD camera mounted at a fixed frame relative to the table. Due to the differences in camera FOVs and the environmental setup, directly applying the video generative model trained on Bridge to our setup does not generalize well. We thus fine-tuned the diffusion model with 20 human demonstrations collected with our setup. In our real-world evaluation, we assume that the target object can be grasped using a top-grasp so that no reorientation of the target object is needed. Note that both the Bridge dataset and our human demonstration datasets do not contain any action label relevant to our robot: Bridge is based on a different robot model and our tabletop videos are human hand manipulation videos.

Results. The predicted object motion qualitative results on the Bridge dataset are presented in Fig. 9. AVDC can reliably synthesize videos, predict optical flow, identify target objects, and infer actions.

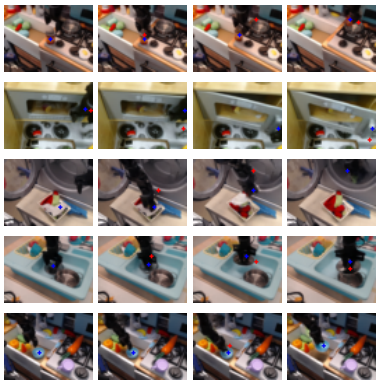

Figure 9: **Qualitative Results on Bridge.** AVDC can reliably infer current subgoals (•) and next subgoals (•) for real-world robot manipulation tasks.

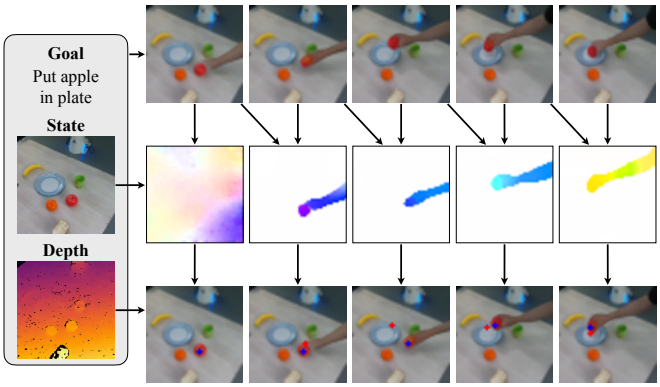

Figure 10: **Qualitative Results on Franka Emika.** AVDC can reliably synthesize a video, predict optical flow between frames, and infer and execute actions to fulfill the assembly task. Current subgoals (•) and next subgoals (•) are rendered in inferred action visualizations.

For the real-world setup, we present screenshots of successful robot trajectories to showcase the practical application of our system. Fig. 10 highlights successful robot trajectories, providing visual evidence of the system's effectiveness in real-world scenarios. We also quantitatively evaluated the success rate of the entire pipeline. In particular, we set up 10 scenes with different initial object configurations and tasks. Each task requires a pick-and-place of an object of a specified category (*e.g.*, apple) to a container (*e.g.*, plate). We show the detailed analysis in Appendix H.

5 Discussion

Limitations. Although our AVDC demonstrates success in diverse simulated and real-world domains, it has several limitations. First, when the majority of an object is occluded by the robot arm, our algorithm may lose track of the object. Moreover, the model can struggle in optical flow prediction under rapidly changing lighting conditions or large object movements in object poses. Additionally, real-world object manipulation requires predicting grasps or contact surfaces for pushing on objects. However, this information isn't directly transferable from real videos due to the disparity between various robot hands and between humans and robots. Therefore, integration of other manipulation algorithms, such as grasp prediction modules (Sundermeyer et al., 2021), is important. Finally, force information, crucial for manipulation, is unobtainable from RGB videos. Future work may consider learning or fine-tuning with real-world interactions to address this.

Conclusion. We have presented an approach to learning to act directly in environments given only RGB video demonstrations. To regress actions, our approach uses dense correspondences between synthesized video frames to infer a transform on objects or surrounding to enact to reach the next synthesized state. We illustrate the general applicability of this approach in both simulated and real-world manipulation and navigation tasks. We further present an open-source implementation for efficient and cheap robot video modeling, enabling effective video policy training in both academic and industry settings. We hope our work inspires further work on learning from videos, which can be readily found on the internet and readily captured across robots.

Bibliography

Shikhar Bahl, Abhinav Gupta, and Deepak Pathak. Human-to-robot imitation in the wild. In *RSS*, 2022. 2

Bowen Baker, Ilge Akkaya, Peter Zhokov, Joost Huizinga, Jie Tang, Adrien Ecoffet, Brandon Houghton, Raul Sampedro, and Jeff Clune. Video PreTraining (VPT): Learning to Act by Watching Unlabeled Online Videos. In Alice H. Oh, Alekh Agarwal, Danielle Belgrave, and Kyunghyun Cho (eds.), *NeurIPS*, 2022. 2

Annie S Chen, Suraj Nair, and Chelsea Finn. Learning Generalizable Robotic Reward Functions from "In-The-Wild" Human Videos. In *RSS*, 2021. 2

Ethan Chun, Yilun Du, Anthony Simeonov, Tomas Lozano-Perez, and Leslie Kaelbling. Local Neural Descriptor Fields: Locally Conditioned Object Representations for Manipulation. In *ICRA*, 2023. 2

Prafulla Dhariwal and Alexander Nichol. Diffusion Models Beat GANs on Image Synthesis. In *NeurIPS*, 2021. 3, 4

Yiming Ding, Carlos Florensa, Pieter Abbeel, and Mariano Phielipp. Goal-Conditioned Imitation Learning. In *NeurIPS*, 2019. 2

Yilun Du, Mengjiao Yang, Bo Dai, Hanjun Dai, Ofir Nachum, Joshua B Tenenbaum, Dale Schuurmans, and Pieter Abbeel. Learning Universal Policies via Text-Guided Video Generation. *arXiv:2302.00111*, 2023. 1, 2, 3, 6

Frederik Ebert, Yanlai Yang, Karl Schmeckpeper, Bernadette Bucher, Georgios Georgakis, Kostas Daniilidis, Chelsea Finn, and Sergey Levine. Bridge Data: Boosting Generalization of Robotic Skills with Cross-Domain Datasets. In *RSS*, 2022. 8

Alejandro Escontrela, Ademi Adeniji, Wilson Yan, Ajay Jain, Xue Bin Peng, Ken Goldberg, Youngwoon Lee, Danijar Hafner, and Pieter Abbeel. Video Prediction Models as Rewards for Reinforcement Learning. *arXiv:2305.14343*, 2023. 2

Bin Fang, Shidong Jia, Di Guo, Muhua Xu, Shuhuan Wen, and Fuchun Sun. Survey of Imitation Learning for Robotic Manipulation. *International Journal of Intelligent Robotics and Applications*, 2019. 2

Chelsea Finn and Sergey Levine. Deep Visual Foresight for Planning Robot Motion. In *ICRA*, 2017. 1, 2

Peter R Florence, Lucas Manuelli, and Russ Tedrake. Dense Object Nets: Learning Dense Visual Object Descriptors By and For Robotic Manipulation. In *CoRL*, 2018. 2

Kaiming He, Xiangyu Zhang, Shaoqing Ren, and Jian Sun. Deep Residual Learning for Image Recognition. In *CVPR*, 2016. 3, 4, 6

Jonathan Ho, Tim Salimans, Alexey Gritsenko, William Chan, Mohammad Norouzi, and David J Fleet. Video Diffusion Models. In *NeurIPS*, 2022. 3

Andrew Jaegle, Felix Gimeno, Andrew Brock, Andrew Zisserman, Oriol Vinyals, and Joao Carreira. Perceiver: General Perception with Iterative Attention. In *ICML*, 2021. 14

Haresh Karnan, Faraz Torabi, Garrett Warnell, and Peter Stone. Adversarial Imitation Learning from Video using a State Observer. In *ICRA*, 2022. 2

Thomas Kipf, Yujia Li, Hanjun Dai, Vinicius Zambaldi, Alvaro Sanchez-Gonzalez, Edward Grefenstette, Pushmeet Kohli, and Peter Battaglia. CompILE: Compositional Imitation Learning and Execution. In *ICML*, 2019. 2

Eric Kolve, Roozbeh Mottaghi, Winson Han, Eli VanderBilt, Luca Weihs, Alvaro Herrasti, Daniel Gordon, Yuke Zhu, Abhinav Gupta, and Ali Farhadi. AI2-THOR: An Interactive 3D Environment for Visual AI. *arXiv:1712.05474*, 2017. 7

Thanard Kurutach, Aviv Tamar, Ge Yang, Stuart J Russell, and Pieter Abbeel. Learning Plannable Representations with Causal InfoGAN. In *NeurIPS*, 2018. 1, 2

Jangwon Lee and Michael S Ryoo. Learning Robot Activities from First-Person Human Videos Using Convolutional Future Regression. In *CVPRW*, 2017. 2

Youngwoon Lee, Andrew Szot, Shao-Hua Sun, and Joseph J. Lim. Generalizable Imitation Learning from Observation via Inferring Goal Proximity. In *NeurIPS*, 2021. 2

Lucas Manuelli, Wei Gao, Peter Florence, and Russ Tedrake. kPAM: KeyPoint Affordances for Category-Level Robotic Manipulation. In *ISRR*, 2022. 2

Suraj Nair, Aravind Rajeswaran, Vikash Kumar, Chelsea Finn, and Abhinav Gupta. R3M: A Universal Visual Representation for Robot Manipulation. In *CoRL*, 2022a. 2

Suraj Nair, Aravind Rajeswaran, Vikash Kumar, Chelsea Finn, and Abhinav Gupta. R3M: A Universal Visual Representation for Robot Manipulation. In *CoRL*, 2022b. 6

Takayuki Osa, Joni Pajarinen, Gerhard Neumann, J Andrew Bagnell, Pieter Abbeel, Jan Peters, et al. An Algorithmic Perspective on Imitation Learning. *Foundations and Trends® in Robotics*, 2018. 2

Jyothish Pari, Nur Muhammad Shafiullah, Sridhar Pandian Arunachalam, and Lerrel Pinto. The Surprising Effectiveness of Representation Learning for Visual Imitation. In *RSS*, 2022. 2

Alec Radford, Jong Wook Kim, Chris Hallacy, Aditya Ramesh, Gabriel Goh, Sandhini Agarwal, Girish Sastry, Amanda Askell, Pamela Mishkin, Jack Clark, et al. Learning Transferable Visual Models From Natural Language Supervision. In *ICML*, 2021. 3, 6

Olaf Ronneberger, Philipp Fischer, and Thomas Brox. U-net: Convolutional networks for biomedical image segmentation. In *Medical Image Computing and Computer-Assisted Intervention*, 2015. 3

Hyunwoo Ryu, Jeong-Hoon Lee, Hong-in Lee, and Jongeun Choi. Equivariant Descriptor Fields: SE(3)-Equivariant Energy-Based Models for End-to-End Visual Robotic Manipulation Learning. In *ICLR*, 2023. 2

Tim Salimans and Jonathan Ho. Progressive Distillation for Fast Sampling of Diffusion Models. In *ICLR*, 2022. 16

Karl Schmeckpeper, Oleh Rybkin, Kostas Daniilidis, Sergey Levine, and Chelsea Finn. Reinforcement learning with videos: Combining offline observations with interaction. In *CoRL*, 2021. 8

Lin Shao, Toki Migimatsu, Qiang Zhang, Karen Yang, and Jeannette Bohg. Concept2Robot: Learning Manipulation Concepts from Instructions and Human Demonstrations. *IJRR*, 40(12-14):1419–1434, 2021. 2

Pratyusha Sharma, Deepak Pathak, and Abhinav Gupta. Third-person visual imitation learning via decoupled hierarchical controller. In *NeurIPS*, 2019. 2

Anthony Simeonov, Yilun Du, Andrea Tagliasacchi, Joshua B Tenenbaum, Alberto Rodriguez, Pulkit Agrawal, and Vincent Sitzmann. Neural Descriptor Fields: SE(3)-Equivariant Object Representations for Manipulation. In *ICRA*, 2022. 2

Anthony Simeonov, Yilun Du, Yen-Chen Lin, Alberto Rodriguez Garcia, Leslie Pack Kaelbling, Tomás Lozano-Pérez, and Pulkit Agrawal. SE(3)-Equivariant Relational Rearrangement with Neural Descriptor Fields. In *CoRL*, 2023. 2

Aravind Sivakumar, Kenneth Shaw, and Deepak Pathak. Robotic Telekinesis: Learning a Robotic Hand Imitator by Watching Humans on Youtube. In *RSS*, 2022. 2

Jiaming Song, Chenlin Meng, and Stefano Ermon. Denoising Diffusion Implicit Models. In *ICLR*, 2021. 16

Lin Sun, Kui Jia, Dit-Yan Yeung, and Bertram E Shi. Human action recognition using factorized spatio-temporal convolutional networks. In *ICCV*, 2015. 4

Priya Sundaresan, Jennifer Grannen, Brijen Thananjeyan, Ashwin Balakrishna, Michael Laskey, Kevin Stone, Joseph E Gonzalez, and Ken Goldberg. Learning Rope Manipulation Policies Using Dense Object Descriptors Trained on Synthetic Depth Data. In *ICRA*, 2020. 2

Martin Sundermeyer, Arsalan Mousavian, Rudolph Triebel, and Dieter Fox. Contact-GraspNet: Efficient 6-DoF Grasp Generation in Cluttered Scenes. In *ICRA*, 2021. 9

Faraz Torabi, Garrett Warnell, and Peter Stone. Behavioral Cloning from Observation. In *IJCAI*, 2018. 2

Faraz Torabi, Garrett Warnell, and Peter Stone. Generative Adversarial Imitation from Observation. In *Imitation, Intent, and Interaction (I3) Workshop*, 2019a. 2

Faraz Torabi, Garrett Warnell, and Peter Stone. Recent Advances in Imitation Learning from Observation. In *IJCAI*, 2019b. 2

Hsiang-Chun Wang, Shang-Fu Chen, and Shao-Hua Sun. Diffusion Model-Augmented Behavioral Cloning. *arXiv:2302.13335*, 2023. 2

Haofei Xu, Jing Zhang, Jianfei Cai, Hamid Rezatofighi, and Dacheng Tao. GMFlow: Learning Optical Flow via Global Matching. In *CVPR*, 2022. 4

Lin Yen-Chen, Pete Florence, Jonathan T Barron, Tsung-Yi Lin, Alberto Rodriguez, and Phillip Isola. NeRF-Supervision: Learning Dense Object Descriptors from Neural Radiance Fields. In *ICRA*, 2022. 2

Tianhe Yu, Deirdre Quillen, Zhanpeng He, Ryan Julian, Karol Hausman, Chelsea Finn, and Sergey Levine. Meta-World: A Benchmark and Evaluation for Multi-Task and Meta Reinforcement Learning. In *CoRL*, 2019. 7

Kevin Zakka, Andy Zeng, Pete Florence, Jonathan Tompson, Jeannette Bohg, and Debidatta Dwibedi. XIRL: Cross-embodiment inverse reinforcement learning. In *CoRL*. PMLR, 2022. 8

Supplementary Material for Learning to Act from Actionless Videos through Dense Correspondences

Table of Contents

A Code

The code for reproducing our results is included in `./codebase_AVDC` directory of the attached supplemental .zip file.

B Extended Qualitative Results

The attached supplemental .zip file contains a web page (index.html), which illustrate the robot execution traces in Meta-World, iTHOR, and our real-world Franka Emika setup. You can also find all supplementary videos and results at https://flow-for-action-from-video.github.io/supplements/.

C Model Architecture and Training Detail

C.1 Text Encoder

We used a fixed pretrained CLIP-Text model for encoding texts. After encoding the texts with CLIP-Text model, we used (Perceiver; Jaegle et al., 2021) as our attention-pooling network to aggregate the output tokens from the CLIP-text model into one single vector and added it to the time embedding of the diffusion model. This simple condition mechanism has been successful in our experiments. We did not use cross-attention on text inputs throughout this work. The hyperparameters of Perceiver are listed in Table 3.

Parameter	Value
depth	2
dim_head	64
dheads	8
dnum_latents	64
dnum_latents_from_pooled	4
dmax_seq_len	512
dff_mult	4

Table 3: Model parameters for our Perceiver.

C.2 Video Diffusion Model

For all models, we use dropout=0, num_head_channels=32, train/inference timesteps=100, training objective=predict_v, beta_schedule=cosine, loss_function=l2, min_snr_gamma=5, learning_rate=1e-4, ema_update_steps=10, ema_decay=0.999. We list all other hyperparameters in Table 4.

	Meta-World	**iTHOR**	**Bridge**
num_parameters	201M	109M	166M
resolution	(128, 128)	(64, 64)	(48, 64)
base_channels	128	128	160
num_res_block	2	3	3
attention_resolutions	(8, 16)	(4, 8)	(4, 8)
channel_mult	(1, 2, 3, 4, 5)	(1, 2, 4)	(1, 2, 4)
batch_size	16	32	32
timesteps	60k	80k	180k

Table 4: Comparison of configuration parameters for Meta-World, iTHOR, and Bridge.

D Additional Ablation Studies

D.1 First-Frame Conditioning

To study the effectiveness of our first-frame conditioning strategy, we conducted a quantitative experiment that compares our RGB-channel-wise concatenating strategy with a trivial baseline: frame-wise concatenate, which concatenates the input frame before the first frame of the noisy video. To evaluate the quality of generated videos, we calculated the mean squared error (MSE) between the GT and the generated last frame. We show the results in Table 5. Each data point is an average MSE calculated with 4000 samples of video generation, and the error bar shows the standard error of MSEs. Our method (cat_c) consistently outperforms frame-wise concatenating (cat_t) in the early stages of training on the Bridge dataset. We also present some qualitative generation results on our website.

We show the average MSE and standard error from 4000 video generation samples below. Since the raw MSE numbers are small, we scaled the numbers by 1000 times for better comprehension.

Training Steps	20000	40000	60000
AVDC (cat_t)	25.17 ± 0.30	20.19 ± 0.28	17.84 ± 0.27
AVDC (cat_c) (Ours)	23.23 ± 0.29	19.30 ± 0.28	17.35 ± 0.26

Table 5: Comparison between different strategies for first-frame conditioning. Our frame-wise concatenating (cat_c) outperforms the alternative models. See text for detail.

Training Steps	20000	40000	60000
AVDC (CLIP)	23.23 ± 0.29	19.30 ± 0.28	17.35 ± 0.26
AVDC (T5-Base)	23.06 ± 0.29	19.10 ± 0.27	17.07 ± 0.26

Table 6: Comparison between different text encoders for the video generation model. Two different text encoders have similar parameter size and have similar performances on our dataset.

D.2 Text Encoder

We compare the video generation quality of our CLIP-text encoder (63M parameters) with the same model but with a T5-base encoder (110M parameters), dubbed AVDC (T5-Base). We used the same pixel-level MSE error as the evaluation metric. Table 6 shows the result. The difference between the performance of the two text encoders is not significant. We also present some qualitative generation results on our website.

E Hardware and complexity analysis

E.1 Training cost

We train all models on 4 V100 GPUs with 32GB memory each. Our claim for training video policies within a day refers to training a diffusion model from scratch on small, environment-specific datasets like in Meta-World and iTHOR experiments. As for a much larger dataset like Bridge, we have to train for longer to obtain consistent results. Despite the large size of Bridge data compared to the datasets we used in the other two experiments, we can generate high-quality and consistent results with just two days of training.

- Meta-World: about 24 hours of training (165 videos)
- iTHOR: about 24 hours of training (240 videos)
- Real world experiment: 48 hours of pretraining on Bridge and 4 hours of fine-tuning on human data. (40000 Bridge + 20 Human videos)

E.2 Inference cost

We conducted our experiments (inference) on a machine with an RTX 3080Ti as GPU. We provide a detailed run time breakdown on Meta-World experiment of each step of our method below.

- **Text-Conditioned Video Generation**: Synthesizing a video of predicted execution is the most time-consuming step of our method, which takes roughly **10.57** seconds (**1.51** seconds per video frame on average).
- **Flow Prediction**: Predicting optical flow between a pair of two subsequent frames takes **0.28** seconds on average.
- **Action Regression from Flows and Depths**: Inferring the action from optical flow prediction **1.31** seconds on average.
- **Action Execution**: Running an inferred action using the controller in the environment takes **1.53** seconds on average.

E.3 Re-planning cost

In Meta-World experiments, AVDC used about 18 seconds for each round of action planning. Since the maximum number of replans is set to 5, the actual number of action planning rounds within an

episode can vary from 1 to 6. That is, the total planning cost ranges from about 18 to 108 seconds on our 3080Ti machine.

E.4 Inference Runtime Improvements

Various techniques can be incorporated into our method to improve its inference efficiency. To speed up the video synthesis step, we can accelerate the sampling process using Denoising Diffusion Implicit Models (DDIM; Song et al., 2021) or progressive distilling the diffusion models for faster sampling (Salimans & Ho, 2022) Also, we can leverage lighter-weight optical flow prediction models to increase efficiency. To accelerate action prediction from flows, we can design more sophisticated techniques for sampling and optimizing actions or parallelizing it using GPUs.

To empirically demonstrate the possibility of significantly improving our method's efficiency, we have conducted an additional experiment that generates videos using DDIM. Instead of iterative denoising 100 steps, as reported in the main paper, we have experimented with different numbers of denoising steps (e.g., 25, 10, 5, 3). We present these qualitative results on out website. We have found that reducing the number of denoising steps to 10 still leads to satisfactory generated video quality, while resulting in a 10x speedup in video generation. Specifically, the overall mean success rate across tasks in Meta-World with 10-step DDIM is **37.5%**, which is competitive with our original method with 100 denoising steps with an overall success rate of **43.1%**. That said, when the task is running time critical, we can speed up the video generation step by ten times with only **5.6%** drop in task performance.

F Meta-World Experimental Setup

This section describes the details for the Meta-World experiments.

F.1 Learning the Diffusion Model

We aim to learn a video diffusion model that can synthesize a video, showing a robot fulfilling a task, from an initial frame and a goal described in natural language. We found that in most goal-conditioned manipulation tasks, the final frame of the whole video is often highly correlated to the text description when the current (first) frame is given. In other words, the model can easily synthesize the last frame given the current frame and text description, while the model is often more uncertain about intermediate frames, and therefore performs poorly on synthesizing intermediate frames.

To take advantage of this finding, we propose an *adaptable frame sampling technique* to sample frames from the whole video for training. In particular, we first randomly sample a frame from the whole video dataset as the current frame. We then uniformly sample $T-2$ frames from the current (*i.e.*, initial) frame to the final frame from the same video. Then, we use these T frames (1 current/initial frame, $T-2$ intermediate frames, and 1 final frame) to train our video diffusion model. We empirically found that this *adaptable frame sampling technique* significantly improves the learning efficiency of the video diffusion model, enabling the training to finish within a single day using just 4 GPUs.

F.2 Calculating Object Rigid Transformations and Inferring Actions

Given the predicted optical flow between each pair of frames of a synthesized video and the initial frame, we aim to infer the actions a robot needs to do to follow the synthesized video.

Tracking Object and Determining Contact Point. Since Meta-World focuses on manipulating objects, we propose to track an object of interest by extracting an object mask. To determine the contact point for the robot to grasp an object, we simply sample $N = 500$ points from the object mask and compute the centroid of an object as the contact point. Note that more sophisticated methods for determining contact points can be employed to further improve the proposed method.

Calculating Object Rigid Transformation Object and Computing Subgoal. Given the optical flow computed from the synthesized video frames, we can use it to compute the 2D correspondence between two frames. We use the RANSAC algorithm to find an optimal 2D transformation that produces the most inliners from the 2d correspondences. We only use these inliner points for the computations in the current and the following steps for better robustness. We apply our method as described in Section 3.3 to obtain a sequence of 3D rigid transformations. Then, we apply these

transformations on the sampled grasp sequentially to obtain a sequence of subgoals, indicating how the object should be moved.

Inferring Actions. Given each subgoal, we decide whether to use "`grasp`" action or "`push`" action to interact with the object by checking if the maximum magnitude of vertical displacement exceeds 10cm based on the heuristic that pick-and-place tasks usually require the robot to lift the object, which produces a vertical displacement; on the other hand, optimal object trajectories of pushing tasks do not exhibit such vertical displacement.

Once we decide if the robot should "`grasp`" or "`push`" the object, we determine the robot arm's action as follows. For the `grasp` mode, we simply control the robot to take a grasping action (closing the grippers) at the grasp point and then move toward the subgoals. For the `push` mode, we put the robot arm in a specific direction to the object that allows pushing before starting to move the robot towards the subgoals. We calculate such direction by extrapolating the line between the grasp point and the first subgoal more than 10cm away from the grasp.

F.3 Replanning Strategy

In Meta-World, we replan (*i.e.*, perform the closed-loop control) by synthesizing a video with the current observed state as the initial frame for the video diffusion model. Then, we use the current object mask and depth information to compute a new sequence of subgoals. Note that we do not re-decide the interaction mode. For the `grasp` mode, we simply move the gripper toward the new subgoals. For the `push` mode, we re-initialize the gripper as described above and then move the gripper toward the new subgoals.

G iTHOR Experimental Setup

G.1 Learning the Diffusion Model

We aim to learn a video diffusion model that can synthesize a video that shows an agent navigating to a target object in first-person point of view in iTHOR indoor scenes. To sample video segments for training, we first randomly sample a frame from the video demonstration dataset, and then we retrieve $T-1$ consecutive future frames from the same video. We do not skip any intermediate frames (*i.e.*, we do not apply the *adaptable frame sampling technique* used in Meta-World). If the number of subsequent frames is less than $T-1$ in the sampled video, we duplicate the last frame to compensate for missing frames. This allows the model to recognize that the target object is found and the agent should stop moving.

G.2 Calculating Scene Transformations and Inferring Actions

Tracking Scene and Calculating Scene Transformation. In the navigation setup, instead of tracking the correspondences of a particular object, we track the correspondences of the entire scene. To this end, instead of generating an object mask, we initialize a scene mask by thresholding out moving points (magnitude of optical flow > 1). Then, to calculate the scene transformation, we apply a similar procedure to the Meta-World experiment for computing the object transformation. However, we do not use the RANSAC algorithm to obtain inliners; instead, at each time step, we simply remove the key points that move out-of-bound (*i.e.*, outside the image) and keep the rest as the inliner points to calculate the scene transformation.

Inferring Actions. Given calculated the scene transformation at each step, we design a procedure to infer an action (`MoveForward`, `RotateLeft`, `RotateRight`, or `Done`). We propose to observe an *imaginary point* located 1 meter in front of the robot. We apply the calculated scene transformation on this *imaginary point*. We then decide the action based on the translation of this *imaginary point* before and after applying the transformation. Specifically, if the translation is close to 0 ($<$ 1mm), since the agent stays still, we choose `Done`. Otherwise, we check the horizontal displacement of this *imaginary point*. If the magnitude of the horizontal displacement is less than 25cm, we choose `MoveForward`. Otherwise, we select `RotateLeft` or `RotateRight` depending on the direction of the displacement.

G.3 REPLANNING STRATEGY

In iTHOR, we replan when we lose tracking of most correspondences from the initial frame. Specifically, if the number of inliners we keep is less than 10% of the original number we sampled, we re-synthesize a video, predict optical flow, and infer actions.

H REAL-WORLD SETUP

Hardware. Our arrangement comprises a Franka Emika robot, and an Intel Realsense D435 RGBD camera mounted at a fixed frame relative to the table. The robot is equipped with a parallel motion two-jaw gripper, and the robot arm is in joint position control mode. Meanwhile, the camera has calibrated intrinsic and extrinsic. Therefore, any object motion predicted in the camera frame can be directly transformed into the world frame.

Dataset Collection. After Bridge dataset training, we finetuned the model with 20 human demonstrations in a real-world tabletop manipulation setting. These videos are collected by humans using their hands to move objects on the table and accomplish tasks. Our object set includes plates, bowls, a few categories of fruits (apples, oranges, bananas, peaches, and mangoes), and utensils such as forks and knives as distractors. The task is to pick up fruits from their initial locations and place them in the specified container (either a plate or a bowl).

Action Prediction and Execution. In our real-world evaluation, we assume that the target object can be grasped using a top-grasp and that no re-orientation of the target object is needed. Therefore, in order to compute the target object poses, we first manually specify the segmentation of the object (in principle, it can be done using other object segmentation models, too), extracts the corresponding optical flow, and compute the sequence of the object poses. We extract its initial pose (in the first frame) and the target pose (in the last frame), and generate a robot arm trajectory using an inverse-kinematics (IK) solver. In practice, we found that since we are using only a small set of tracking points (objects are small in our camera view), the reconstruction of 3D rotations is not robust. This can be potentially addressed by leveraging a higher-resolution video generative model or simply, different camera configurations.

Failure Mode Analysis In our real-world experiments, we found that our approach failed in 8 of the 10 tested trials. We found 75% of the failures were caused by the wrong plan from video diffusion model. It either picked the wrong object or placed at the wrong target. The other 25% of the failures were caused by the discontinuity of video generation. The generated plan seems to be correct, but the object disappeared in some intermediate frame, which eventually led to the failure.